https://doi.org/10.20965/jdr.2019.p0687

Paper:

Tracing Volcanic Activity Chronology from a Multiparameter Dataset at Shinmoedake Volcano (Kirishima), Japan

Taishi Yamada[*,†], **Hideki Ueda**[*], **Toshiya Mori**[**], **and Toshikazu Tanada**[*]

[*]National Research Institute for Earth Science and Disaster Resilience (NIED)
3-1 Tennodai, Tsukuba, Ibaraki 305-0006, Japan
[†]Corresponding author, E-mail: taishi@bosai.go.jp
[**]Geochemical Research Center, Graduate School of Science, The University of Tokyo, Tokyo, Japan

[Received January 4, 2019; accepted July 12, 2019]

Routine volcano monitoring increasingly involves multiparameter datasets. Databases that include multidisciplinary datasets have great potential to contribute to the evaluation of ongoing volcanic eruptions and unrest events. Here, we examine the characteristics of a multiparameter dataset from Shinmoedake volcano (Kirishima) in Japan for the period of 2010–2018 to examine how the chronology of volcanic activity can be traced. Our dataset consists of global navigation satellite system (GNSS), seismic, tilt, infrasound, sulfur dioxide (SO_2) column amount, and video records. We focus mainly on the period after 2012, particularly a series of ash emissions in 2017 (hereafter the 2017 eruption), lava effusion, and Vulcanian eruptions in 2018 (hereafter the 2018 eruption). Our dataset shows that the GNSS observations successfully captured the gradual inflation of the volcano edifice, suggesting magma intrusion or pressure buildup in the magma storage region prior to the 2017 and 2018 eruptions. The number of volcanic earthquakes also gradually increased from 2016 toward the eruptions, particularly events occurring beneath Shinmoedake. Tilt data captured a precursor tilt event prior to the 2017 eruption and a magma chamber deflation during the lava effusion of the 2018 eruption. Tilt, seismic, infrasound, SO_2 gas column, and video data record signals accompanying periodic degassing during the lava effusion and explosive degassing accompanying the Vulcanian eruptions, which have similar characteristics to those reported for past eruptions at Shinmoedake and other volcanoes. This similarity suggests that multidisciplinary databases will be an important reference for future evaluations of ongoing volcanic activity and unrest.

Keywords: volcanic eruption, database, eruption chronology, Shinmoedake, Kirishima

1. Introduction

A number of volcano observatories now deploy multiparameter networks at active volcanoes, i.e., a combination of multi-disciplinary observation techniques such as seismic, geodetic, infrasonic, visual, infrared, volcanic gas, etc. [1]. Previous studies have demonstrated that multiparameter observations are effective in understanding volcanic activity dynamics in ways that cannot be inferred from single-discipline observations (e.g., [2–5]). As amount of observational monitoring data has significantly grown, some efforts have been made to construct multiparameter monitoring data databases for volcanoes [6, 7]. The aim of these databases is to assist in ongoing volcanic activity evaluation and eruption forecasting, by comparing data from current unrest/activity to the characteristics of that accompanying past unrest/activity and from other volcanoes that show similar behavior (analog volcanoes) [8]. Therefore, it is essential to comprehend the characteristics of accumulated data in an individual and a global database to contextualize any new eruption or unrest. Pioneering works in volcano seismology showed that the types of volcanic earthquakes can be useful to evaluate the current state of active volcanoes and forecasting eruptions based on conceptual magma ascent models (e.g., [9–14]). Geodetic observations have also captured a variety of precursor signals of eruptions (e.g., [15–17]). However, no one dataset captures the full breadth of processes that are involved in transporting magma from a lower crust magma reservoir to the surface, and given the current more abundant multiparameter observations and datasets, it is imperative to employ a more comprehensive interpretation methodology to understand volcanic activity using these multiparameter datasets. In other words, it is important to organize which aspect of volcanic activity can be obtained and comprehended by each observation method and corresponding data to understand their strengths and limits and use them collectively in appropriately weighted schema.

The multiparameter dataset from Shinmoedake volcano in Japan during the period of 2010–2018 provides a unique opportunity to examine how one can trace the eruption chronology using a multiparameter database. We investigated the important characteristics of the dataset and the relationship of each monitoring dataset with the corresponding volcanic activity chronology. Detailed analyses of each dataset will be completed in future research articles that will examine the dynamics behind the

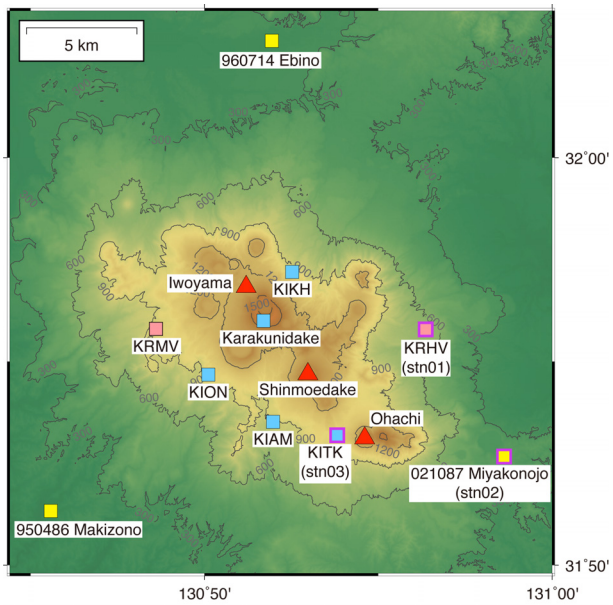

Fig. 1. Observation networks at the Kirishima volcano complex. Red triangles show location of Shinmoedake and Iwoyama volcanoes. Pink, sky, and yellow squares denote permanent stations of the NIED (V-net), JMA, and GSI (GEONET), respectively. Stations with violet lines have co-located SO_2 column measurement system operated by the Geochemical Research Center of the University of Tokyo.

characteristics found to correlate with eruption activity.

2. Shinmoedake and Available Datasets

2.1. Shinmoedake Volcano

The Kirishima volcano complex is on the southern Kyusyu Island of Japan, and composed of more than 25 andesitic stratovolcanoes and two calderas [18]. During the last decade, the most active volcano in the Kirishima area has been Shinmoedake (**Fig. 1**). During the last 300 years, Shinmoedake has erupted in 1716–1717, 1822, 1952, and 2011 [19]. The climax of the 2011 eruption consisted of three sub-Plinian eruptions, and subsequent lava effusion followed by intermittent Vulcanian eruptions [20, 21]. Shinmoedake is not the only active volcano in the Kirishima complex (**Fig. 1**). Ohachi volcano had a series of Vulcanian eruptions up to 1923 [22]. Iwoyama volcano had a small phreatic eruption on April 19, 2018 [23]. According to geologic study, Iwoyama had two eruption activities during the period 1300–1500 and 1500–1700 [24]. We mainly focused on the volcanic activity of Shinmoedake following the 2011 eruption and leading up to the 2017 and 2018 eruptions.

2.2. Available Datasets

Our dataset consists of observational data obtained by the National Research Institute for Earth Science and Disaster Resilience (NIED), the Japan Metrological Agency (JMA), the Geospatial Information Authority of Japan (GSI), and the Geochemical Research Center of the University of Tokyo. We describe the observation networks of each organization in the following. Details of the instruments and sampling rates of each network are summarized in **Table 1**.

The NIED operates two permanent stations in the Kirishima complex (V-net, **Fig. 1**) [25]. We use the continuous data recorded by borehole short-period seismometers (V225 and V224, Mitsutoyo), borehole pendulum-type tiltmeters (JTS-3B, Mitsutoyo), and Global Navigation Satellite System (GNSS) receivers (Delta-G3T and RingAnt-DM, Javad). We used the NIED volcanic earthquake hypocenter catalog for the Kirishima complex, which has been determined using seismic data from both the NIED and JMA since February 2011.

The JMA network in the Kirishima complex consists of more than 40 stations [26]. We used data recorded by a borehole short-period seismometer (V225 and V224, Mitsutoyo) at KITK, borehole tiltmeters (JTS-33, Mitsutoyo) at KITK, and KION, infrasound microphones (ACO 3348, Aco) at KIAM, KION, and KIKH, and video image data from Karakunidake (**Fig. 1**).

The GSI operates a nationwide GNSS network, GEONET [27]. We examine the GNSS data recorded at three of the GEONET stations: 960714 (Ebino), 021087 (Miyakonojo), and 950486 (Makizono) (**Fig. 1**).

Since November 2017, the Geochemical Research Center of the University of Tokyo has operated a continuous sulfur dioxide (SO_2) column amount measurement network using differential optical absorption spectroscopy (DOAS) [28–31] at three stations: co-located with stations KRHV (stn01), 021087 (stn02), and KITK (stn03) (**Fig. 1**). The DOAS measurement system consists of a miniature ultraviolet (UV) spectrometer (FLAME-S, Ocean Optics), a 1–1.5-m-long optical fiber ($\phi = 600\ \mu$m), a collimator lens with a visible light cut filter (U-330, Hoya), and a compact Internet of Things device (Plat Home).

3. Time Series of Data During 2010–2018

3.1. 2010–2018 General Trends

Figure 2(a) shows the temporal change in horizontal baseline lengths for the four GNSS station pairs from April 2010 to July 2018 (all dates and times are Japanese Standard Time (JST)). As reported by previous authors, all baseline length data show changes in the ground deformation of the volcano edifice related to volcanic activity. For the 2011 eruption, horizontal baseline lengths show inflation, deflation accompanying sub-Plinian eruptions and lava effusion of the 2011 eruption, followed by re-inflation until 2012 [32–35]. During the period from 2012 to late 2013, all baseline lengths were nearly constant. Then, beginning in early 2014, three of the four pairs (KRHV-KRMV, Ebino-Miyakonojo, and Ebino-Makizono) began to extend again. The baseline lengths for Ebino-Miyakonojo and Ebino-Makizono showed a

Table 1. Details of the instruments of each observation network in the Kirishima area.

Seismometer	Station	Instrument	Sampling frequency	Natural period
	KRHV, KRMV, and KITK	V225 and V224 (Mitsutoyo)	100 Hz	1 s
Tiltmeter	Station	Instrument	Sampling frequency	
	KRHV and KRMV	JTS-3B (Mitsutoyo)	20 Hz	
	KITK and KION	JTS-33 (Mitsutoyo)	1 Hz	
Infrasound microphone	Station	Instrument	Sampling frequency	Flat response
	KIAM, KION, and KIKH	ACO 3348 (Aco)	100 Hz	0.1–100 Hz
GNSS	Station	Receivers	Anttena	
	KRHV and KRMV	DELTA-G3T (Javad)	RingANt-DM (Javad)	
	960714, 210870, and 950486			
Video	Station	Instrument	Effective megapixels	
	Karakunidake	PTC-113 (Mikami)	38	
DOAS	Station	UV spectrometer	Collimator lens	Sampling frequency
	stn01, stn02, and stn03	FLAMES-S (Ocean optics)	U-330 (Hoya)	0.1 Hz

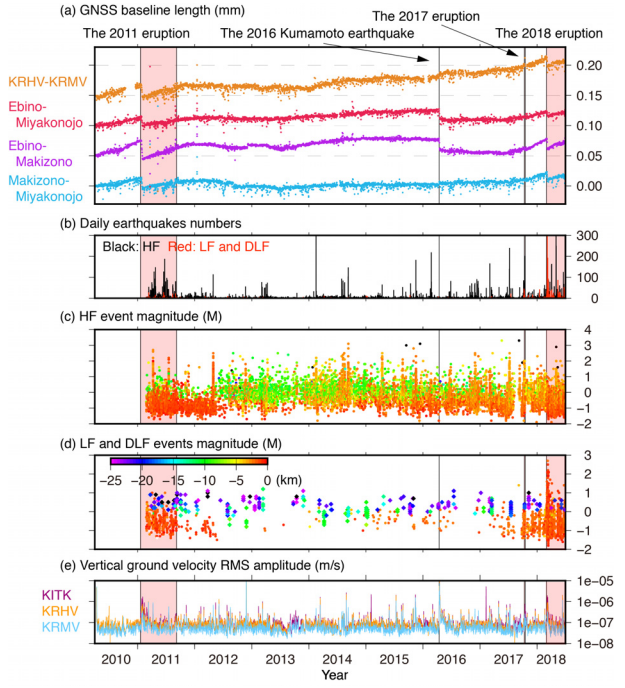

Fig. 2. Time series of dataset during the period 2010–2018. (a) One-day average baseline lengths of the GNSS station pairs in the Kirishima area. (b) Daily number of volcanic earthquakes in the Kirishima area routinly processed by the NIED since February 2011. (c) Magnitude of HF event of volcanic earthquakes. The color of each plot denotes the focal depth following a scale shown in (d). (d) Magnitude of LF (dot) and DLF (diamond) events of volcanic earthquakes. (e) RMS amplitude of daily average vertical ground veclocity.

step-like signal on April 16 2016, induced by the coseismic deformation of the Kumamoto earthquake [36]. Contraction of the baseline lengths of these two pairs for one year after the earthquake may have been because of post-seismic deformation [37]. From the middle of 2017, all baseline lengths showed considerable extension. On October 11, 2017, a series of ash emission events began at Shinmoedake, and lasted for 6 days [38], however, the baseline lengths do not show any considerable changes accompanying the 2017 eruption. During the period of March 6–9, 2018, all baseline lengths showed a step-like contraction, accompanying lava effusion at the summit of Shinmoedake [39]. Following the effusive eruption, all baseline lengths began to show extension once again. This deformation cycle associated with the 2018 eruption is similar to that in the case of the 2011 eruption.

Figure 2(b) shows the daily number of volcanic earthquakes routinely processed by the NIED. The NIED divides earthquakes into four event types based on frequency and focal depth criteria. Events having a peak frequency between 9–10 Hz are High Frequency (HF), 2–3 Hz are Low Frequency (LF), 4–8 Hz are Intermediate Low Frequency (ILF), and $<$ 8 Hz with a focal depth mainly between 10–25 km are Deep Low Frequency DLF (e.g., [40]). For simplicity, in the present study we grouped LF and ILF together as LF events. Temporal changes in the magnitude of HF, LF, and DLF events are shown in **Figs. 2(c)** and **(d)**. **Fig. 3** shows the epicenters of all events during each year from 2011 to 2018. The color of the points in **Figs. 2(c)**, **2(d)**, and **3** corresponds to the focal depth. From these figures, we see that in 2011 there are two major seismic zones: beneath Shinmoedake, and about 7 km to the north-west of Shinmoedake, near the geodetically modelled [32, 34] magma chamber of the 2011 eruption. These events have a focal depth shallower than 5 km. The seismicity of the latter area may also represent microearthquakes related to local faults and the Ogiri Geothermal Power Plant [41] as operation of geothermal power stations can induce local seismicity (e.g., [42, 43]). The number of shallow events

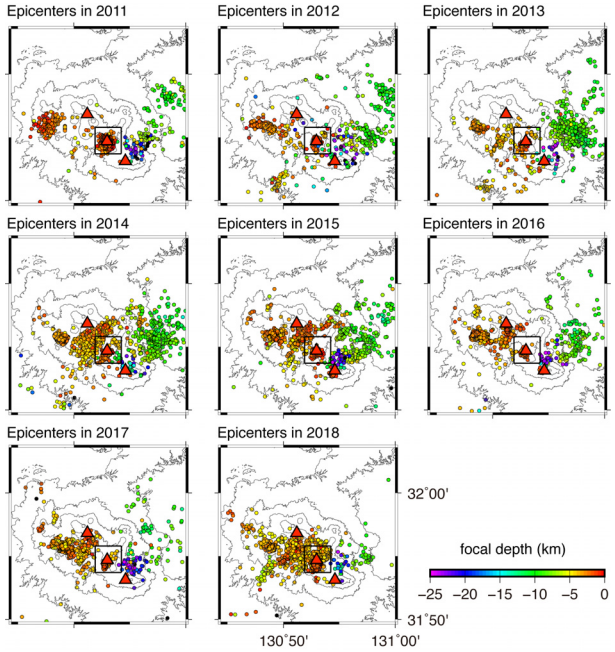

Fig. 3. Epicenter distribution of volcanic earthquakes in the Kirishima area routinely processed by the NIED during each year from 2011 to 2018. Red triangles correspond to the location of Shinmoedake and Iwoyama volcanoes.

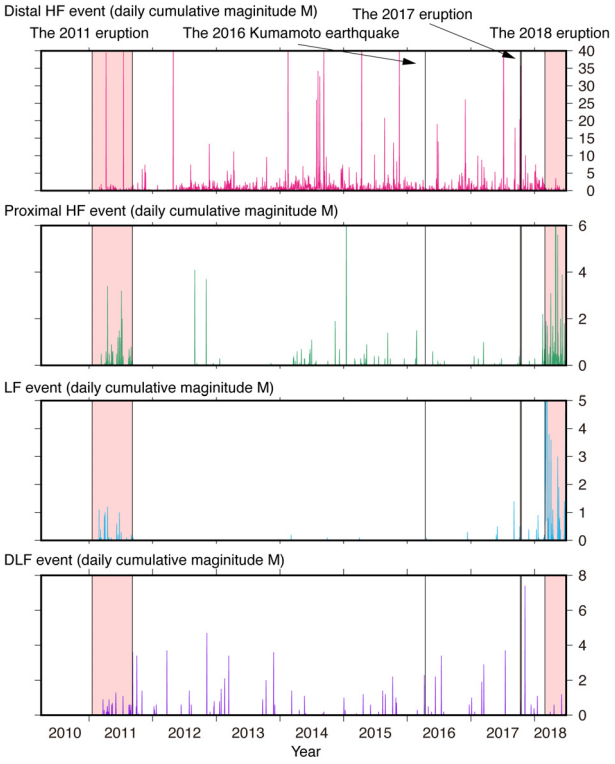

Fig. 4. Time series of the 1-day cumulative magnitude of distal HF, proximal HF, LF, and DFL events during the period of 2010–2018.

gradually decreased from mid-2011 (**Figs. 2(b)** and **(c)**). Instead, a number of HF events at a focal depth of approximately 10 km (green color) dominate from 2012. These HF events have epicenters in the eastern Kirishima area (**Fig. 3**). Simultaneously, epicenters of shallower events (red color) began to gradually scatter from Shinmoedake and the inferred magma chamber. LF events at a depth greater than 20 km also constantly occurred in south-east of Shinmoedake (**Figs. 2(c)** and **3**). From 2015, the number of HF events at a shallow depth ($<$ 5 km) increased again. The change may partly represent active seismicity at Iwoyama [23]. During 2017, the number of HF events at 10 km depth significantly decreased and the number of LF events gradually increased (**Figs. 2(b)** and **(c)**). The seismicity of LF events continued after the 2017 eruption. Lava effusion of the 2018 eruption was accompanied by a number of syn-eruptive LF events (**Fig. 2(c)**).

In addition to the classification by the NIED, we divided HF events into proximal and distal events following the conceptual idea of White and McCausland [12], to examine the seismicity in the Kirishima volcano complex in detail. We defined an HF event occurring beneath Shinmoedake (in the square in **Fig. 3**) as a proximal HF event, and in another area as a distal HF event. **Fig. 4** shows the time history of the 1-day cumulative magnitude of distal HF, proximal HF, LF, and DLF events in the same time window as that of **Fig. 2**. We calculated the 1-day cumulative magnitude using events having a magnitude greater than 0. Most LF events in our catalog had epicenters within the proximal range shown in **Fig. 3**. The activity during 2011 and following quiescence of the seismicity beneath Shinmoedake is clearly recognized in **Fig. 4**. During the period 2012–2017, **Fig. 4** shows distal HF events dominant as shown in **Figs. 2** and **3**. Some swarms of LF events are recognized before the 2017 eruption and at the beginning of the 2018 eruption. Swarms of DLF events are intermittently occurred during this period.

Figure 2(e) shows the daily average of the Root Mean Square (RMS) amplitude of the vertical ground velocity recorded at KITK, KRHV, and KRMV. The RMS amplitudes showed significant increases accompanying the 2011 eruption, the Kumamoto earthquake, the 2017 eruption, and the 2018 eruption. However, no considerable gradual temporal change of the RMS amplitude at a time scale of several years was discerned.

We next set the time window to 1.5 years including the 2017 and 2018 eruptions (**Fig. 5**). Temporal changes in the baseline lengths of the GNSS data during the period from January 2017 to August 2018 are shown in **Fig. 5(a)**. The periods highlighted in pink correspond to the 2017 and 2018 eruptions [23, 38]. The characteristics of the baseline length change are basically the same as those shown in **Fig. 2(a)**. It is evident that baseline lengths extension accelerates following the 2017 eruption.

Figure 5(b) shows the daily average value of tilt data at KRHV and KRMV. The gray-shaded periods correspond to times when the instrument at KRHV was not operational due to mechanical issues. A step-like signal occurred during March 2018 coincides with and similar to the characteristics of the GNSS baseline length data (**Fig. 5(a)**). However, because of their sensitivity, the tilt

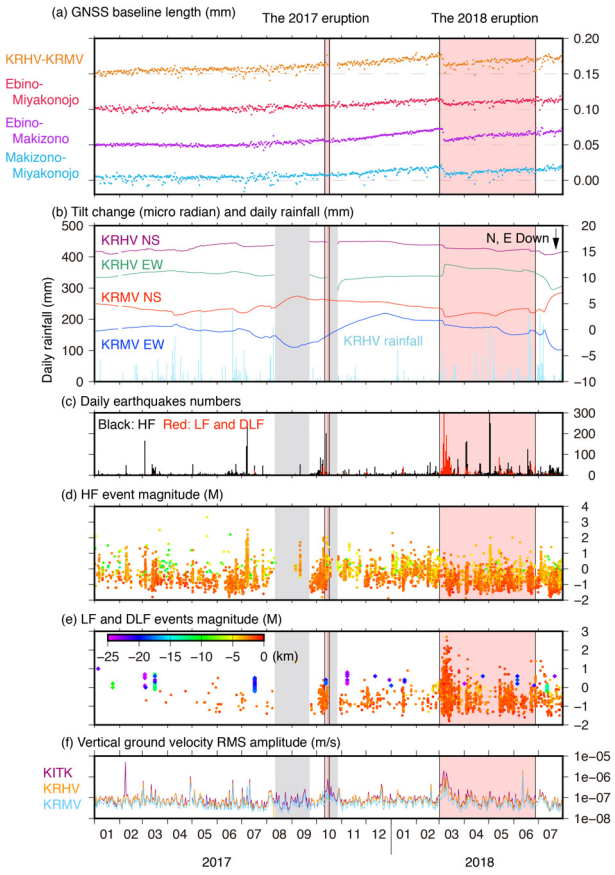

Fig. 5. Time series of dataset during the period from January 2017 to July 2018. The periods of the 2017 and 2018 eruptions are shown in pink. Gray-shaded periods correspond to the period when the instruments at KRHV were not operational and the earthquake catalog has few data. (a) 1-day average baseline lengths of the GNSS station pairs in the Kirishima area. (b) Daily average of tilt records at V-net and rainfall data at KRHV. (c) Daily number of volcanic earthquakes in the Kirishima area from the volcanic earthquake catalog of the NIED. (d) Magnitude of HF event of volcanic earthquakes. The color of each plot denotes the focal depth following a scale shown in (e). (e) Magnitude of LF (dot) and DLF (diamond) events of volcanic earthquakes. (f) RMS amplitude of daily average vertical ground veclocity.

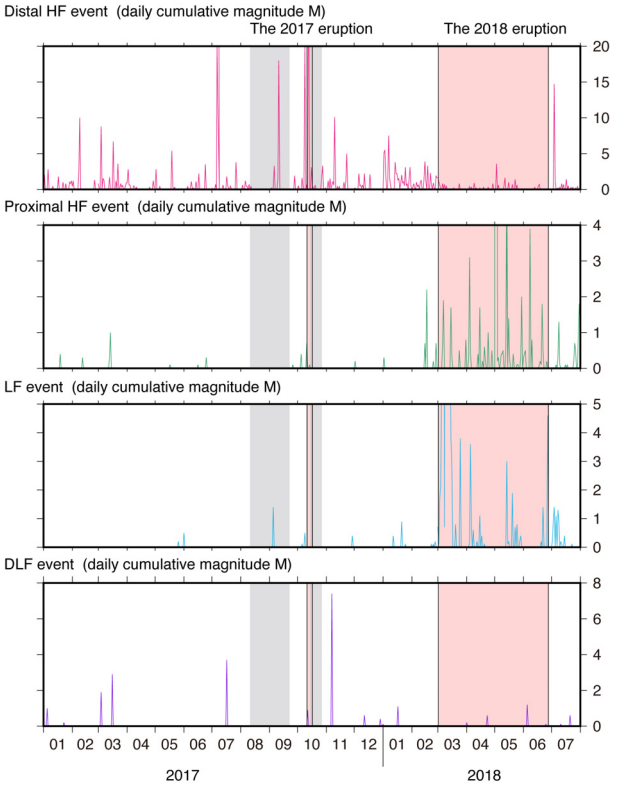

Fig. 6. Time series of the 1-day cumulative magnitude of distal HF, proximal HF, LF, and DFL events during the period from January 2017 to July 2018.

data also show some signals not associated with Shinmoedake eruptions. Borehole tiltmeters can have a resolution on the order of nano-radians for ground deformation which is much more sensitive than that of the GNSS measurements which have a resolution on the order of several centimeters [44]. Tiltmeters, even in boreholes, record more localized deformation than that GNSS is typically capable of resolving. Therefore, the tiltmeters will record ground deformation that is unrelated to volcanic activity [45], or highly localized to only be recorded on one or two instruments. A potential noise source for borehole tilt data is a change in the movement of ground water [46]. We also plotted daily rainfall data at KRHV as shown in **Fig. 5(b)**. For instance, tilt changes during April, May, June, and July of 2017 and May, June, and July of 2018 may be because of underground water movement caused by heavy rainfall.

Figures 5(c), **(d)**, and **(e)** show the daily numbers and magnitude of HF and LF events. As in **Fig. 2**, the color of each dot denotes the focal depth in **Figs. 5(d)** and **(e)**. The catalog of volcanic earthquakes shows few data points during the gray-shaded period, as the hypocenter accuracy was poor because of the lack of data at KRHV. As shown in **Fig. 6**, we plotted the 1-day cumulative magnitude of distal HF, proximal HF, LF, and DLF events in the same time window as that shown in **Fig. 5**. We recognized an increase in swarms of distal HF and DLF events during June 2017, and an increase in proximal HF and LF events prior to the onset of the 2017 eruption. The number of shallow LF events significantly increased following the onset of the 2018 eruption, corresponding to the lava effusion at Shinmoedake starting on March 6 (**Figs. 5** and **6**).

Figure 5(f) shows the daily RMS amplitude of vertical ground velocity at KITK, KRHV, and KRMV during this period. An increase in the RMS amplitude accompanied the 2017 eruption and the step-like ground deformation during the 2018 eruption. However, as well as in **Fig. 2(e)**, any considerable temporal change is not evident at the time scale of several months to 1 year.

3.2. The 2017 Eruption

Next, we focus on data accompanying the 2017 eruption. Tilt records in the period from October 7 to 18,

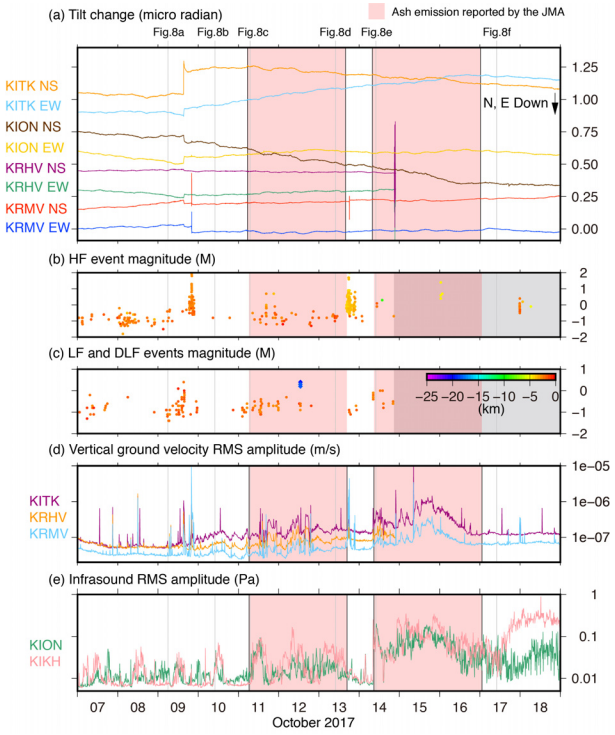

Fig. 7. Time series of dataset during the period October 7–18, 2018. The periods in pink correspond to the duration of ash emissions from Shinmoedake reported by the JMA [32]. (a) Tilt records without tidal components. (b) Magnitude of the HF events of volcanic earthquakes. The color of each plot denotes the focal depth following a scale shown in (c). (c) Magnitude of the LF events of volcanic earthquakes. (d) RMS amplitude of the 10-min average of vertical ground veclocity. (e) The RMS amplitude of the 10-min average of infrasound records.

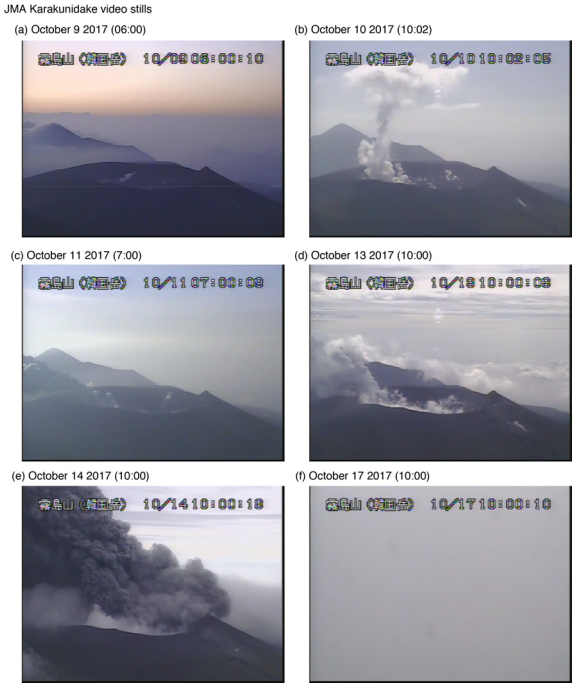

Fig. 8. Still images of video data from Karakunidake station of the JMA during the 2017 eruption. (a) At 06:00 on October 9. (b) At 10:02 on October 10. (c) At 07:00 on October 11. (d) At 10:00 on October 13. (e) At 10:00 on October 14. (f) At 10:00 on October 17.

2018 are shown during **Fig. 7(a)**. Periods of highlighted in pink are those of continuous ash emissions [38]. Here, the tidal components have been removed using BAYTAP-G [47]. During this period, the north-south (NS) component of the tilt at KRMV records a considerable linear trend (**Fig. 5(b)**). Therefore, the trend was removed by using the trend from the data before this period shown in **Fig. 7** (October 2–7). **Fig. 8(a)** shows a still from a video of Shinmoedake at 06:00 on October 9 taken from the Karakunidake station. Small fumaroles are seen in the crater of Shinmoedake. **Figs. 7(b)** and **(c)** show the time series of the magnitudes of the HF and LF events. The timing of **Fig. 8(a)** corresponds to when the number of LF events began to increase. At approximately 15:10 on October 9, a step-like tilt change was recorded at all stations. The largest tilt change was a northward uplift at KITK (**Fig. 7(a)**), the closest station to Shinmoedake. A swarm of LF events accompanied the tilt event (**Fig. 7(c)**). From **Fig. 7(b)**, a swarm of HF events occurred at approximately 18:40. However, this swarm was associated with a tilt change only at KRMV and detailed examinations are needed to interpret such a localized event. The RMS amplitude (10-min averages) of vertical ground velocity shows that a considerable increase in seismic amplitude was recorded with these two tilt events (**Fig. 7(d)**). Another remarkable characteristic of the RMS amplitude data is the amplitude ratio between that at KITK and at KRHV. Prior to October 9, the RMS amplitudes at KITK (V_{KITK}) and KRHV (V_{KRHV}) were nearly the same. For example, the RMS amplitudes at both stations were $V_{\mathrm{KITK}} = 5.17 \times 10^{-8}$ m/s and $V_{\mathrm{KRHV}} = 5.24 \times 10^{-8}$ m/s at 00:00 on October 9. However, the amplitude at KITK increases to a higher value than that of KRHV following the tilt events. At 00:00 on October 10, the RMS amplitudes were $V_{\mathrm{KITK}} = 9.76 \times 10^{-8}$ m/s and $V_{\mathrm{KRHV}} = 5.06 \times 10^{-8}$ m/s. **Fig. 8(b)** shows a still image of Shinmoedake on October 10 (10:02). The maximum height of the fumaroles from the crater is considerably greater than that on October 9 (**Fig. 8(a)**). According to the JMA [38], ash emissions begin at 05:34 on October 11. The ash emissions from the crater can be seen in a still image at 07:00 (**Fig. 8(c)**). **Figure 7(e)** shows the RMS amplitude (10-min averages) of infrasound data at KION and KIKH. Infrasound data at KIAM was not used here because of heavy noise. During the period of October 7–12, the infrasound RMS amplitudes varied within a range of 0.01–0.1 Pa. The source of the fluctuation signals may be from artificial noise or wind. From **Fig. 7(e)** signals from ash emissions from October 11 cannot be identified. The JMA [38] reported that ash emissions stopped on October 13, and restarted on October 14. The second ash emissions stopped on October 17 (00:30). Video images at Karakunidake recorded the repose of the ash emissions (**Fig. 8(d)**) and the second ash emissions (**Fig. 8(e)**).

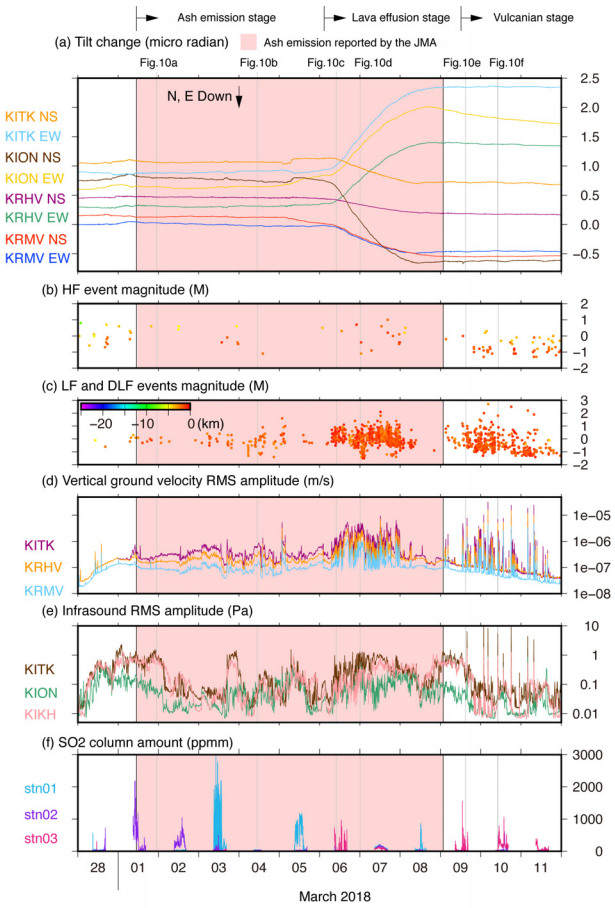

Fig. 9. Time series of dataset during the period from Febrary 28 to March 11, 2018. The period in pink corresponds to the duration of ash emissions from Shinmoedake reported by the JMA [18]. (a) Tilt records without the tidal components. (b) Magnitude of the HF events of volcanic earthquakes. The color of each plot denotes the focal depth following a scale shown in (c). (c) Magnitude of the LF events of volcanic earthquakes. (d) RMS amplitude of the 10-min average of vertical ground veclocity. (e) RMS amplitude of the 10-min average of infrasound records. (f) Sulfer dioxide column amount change with time.

The RMS amplitude of the seismic and infrasound signals shows a peak on October 15. The seismic amplitude gradually decreased and reached a flat level on October 17 (**Fig. 7(d)**). Tilt records of the east-west (EW) component at KITK and the NS component at KION show a continuous tilt trend following the tilt event on October 9, while those of the other stations are flat. This signal stopped on October 16. The decrease in seismic amplitudes and cessation of the tilt change on October 16 can be related to the end of the ash emissions.

3.3. The 2018 Eruption

Figure 9(a) shows time histories of the tilt from February 28 to March 11, 2018. Tidal components were removed from all tilt records using BAYTAP-G [47]. The period highlighted in pink is that of continuous ash emissions from March 1 to 9, as reported by the JMA [23]. Although a slight tilt change was recorded prior to the onset of ash emissions on March 1, it is not evident that this signal is related to volcanic activity from **Fig. 9(a)**. **Figs. 9(b)** and **(c)** show the magnitudes of HF and LF events. From this time window, we see no particular change in the HF events is associated with the onset of the ash emissions. The number of LF events gradually increased from March 1, the onset of the ash emissions. The RMS amplitude (10-min averages) of the vertical ground velocity at KITK, KRHV, and KRMV was shown in **Fig. 9(d)**. An increase in the RMS amplitude was recorded at approximately 10:00 on March 1 as a result of an increase in tremors and LF events. Simultaneously, the amplitude at KITK began to increase relative to that at KRHV, as in the case of the 2017 eruption, which means the source of the seismic wave was possibly around Shinmoedake. The JMA [23] reported the first ash fall near Shinmoedake at approximately 11:00 on March 1. **Fig. 9(e)** shows time series of the infrasound RMS (10-min averages) amplitudes at KITK, KION, and KIKH. No obvious signal corresponding to the onset of the ash emissions is seen due to poor signal-to-noise ratio. In contrast, a remarkable increase in the SO_2 column amount was observed at approximately 10:00 at stn02 (**Fig. 9(f)**). A peak in the SO_2 column amount on March 1 corresponded to the peak of the seismic RMS amplitudes (**Fig. 9(d)**). Though not shown here, the summit of Shinmoedake was covered with clouds at that time and the video images from Karakunidake did not record the crater surface. A still image of Shinmoedake at 23:00 on March 1 is shown in **Fig. 10(a)** which captures the ongoing ash emissions from the crater. The ash emissions continued on March 4 (**Fig. 10(b)**). On March 6, a considerable tilt change appeared as shown in **Fig. 9(a)** with an amplitude of the order of several micro radians. The polarity of these records was nearly the same as the syn-eruptive tilt changes during sub-Plinian and lava effusion events during the 2011 eruptions, which are modeled by a spherical pressure source at 7 km northwest of Shinmoedake [32]. At the same time, the number and magnitude of the LF events significantly increased (**Figs. 9(c)** and **6**). Simultaneously, the seismic RMS amplitude began to show a disturbance (**Fig. 9(d)**). The time series of infrasound RMS amplitudes also show a similar shaped change in signal to that in the seismic RMS amplitude, although the amplitudes of the infrasound signals are within the range of the background noise level (**Fig. 9(e)**). As a representative of these signals, we plotted 1-h raw traces of vertical ground velocity at KRHV, infrasound at KIAM, and RMS amplitudes (1-min average) of both records as shown in **Fig. 11(a)**. The seismogram recorded LF and tremor events. Infrasound pulses accompanied these tremors and some LF events. From **Fig. 11(a)**, increases in the RMS amplitudes mainly reflected the occurrence of tremors, rather than LF events. **Fig. 11(b)** shows the raw vertical ground velocity and normalized power spectral density of the LF events shown in **Fig. 11(a)**. Most LF events had a peak frequency of 1.1 Hz. We also plotted the normalized power spectral density of a tremor (an event surrounded

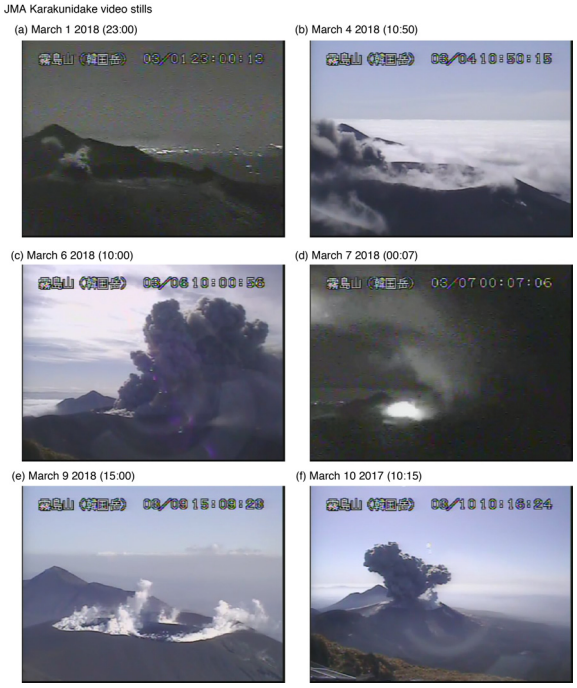

Fig. 10. Still images from video data at the Karakunidake station of the JMA during the 2018 eruption. The angle of view is occasionally changed for monitoring purposes. (a) At 23:00 on March 1. (b) At 10:50 on March 4. (c) At 10:00 on March 6. (d) At 00:07 on March 7. (e) At 15:00 on Match 9. (f) At 10:15 on March 10.

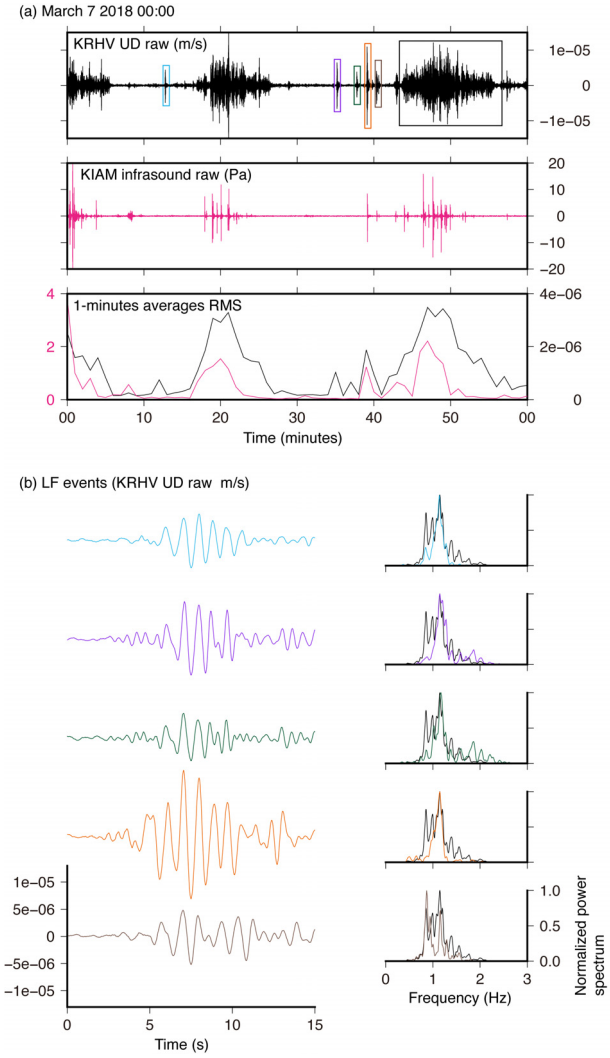

Fig. 11. (a) Raw vertical ground velocity at KRHV, infrasound waveforms at KITK, and the 1min-average RMS amplitudes of each trace for 1 h from 00:00 on March 7, 2018. (b) Raw vertical ground velocity traces of LF events at KRHV and the normalized power spectral density. The color of each event corresponds to the squares in the 1-h trace in (a). The normalized power spectral density of a tremor event in (a) (black squares) is shown by the black line.

by a black square in **Fig. 11(a)**). One of the dominant frequencies of the tremor corresponds to that of LF events, suggesting that they share similar source mechanism.

The overall size of the ash cloud from the vent at 10:00 on March 6 (**Fig. 10(c)**) was much greater than that shown in **Figs. 10(a)** and **(b)**. At midnight (00:07) on March 7, a still image captured a glow from the crater (**Fig. 10(d)**).

We examined in detail the signals on March 6 by plotting the tilt data (**Fig. 12(a)**), 1-min RMS average of the seismic amplitudes (**Fig. 12(b)**), and 1-min RMS average of the infrasound RMS amplitudes (**Fig. 12(c)**) as well as the SO_2 gas column amount (**Fig. 12(d)**) for 4 h (starting at 12:00). The tilt records shown in **Fig. 12(a)** are filtered within the frequency band from 5.0×10^{-4} to 4.0×10^{-3} Hz using an acausal filter to focus on higher frequency signals than those that are dominant in this time window (**Fig. 9(a)**). A periodic ground deformation signal in the filtered tilt records appears, as well as coincident increases and decreases in the seismic and infrasound RMS amplitudes, indicating that the source process for both is the same. The NS component at KITK shows the largest tilt amplitude. We emphasize the period when the signal at KITK shows a southward uplift in gray highlight in **Fig. 12**. The increasing seismic and infrasound RMS amplitudes are coincident with the southward uplift of KITK. Because KITK is to the southeast of Shinmoedake, southward uplift may be due to deflation of the edifice of Shinmoedake. The SO_2 column amount at stn03 also showed some periodic increases during this period (**Fig. 12(d)**). An approximately 10-min time shift between each SO_2 column amount peak and immediately before the seismic and infrasound RMS peaks. If we assume that the increases in the SO_2 column amount capture the volcanic gas emitted from Shinmoedake, **Fig. 12** suggests that the average diffusion velocity of the gas was approximately 10 m/s considering the horizontal distance between Shinmoedake and stn03 (KITK) of 3.1 km. Although this estimation is approximate, it is consistent with the wind direction of SSE at 14:00 at Mizobe, approximately 19 km from Shinmoedake [48], and an average wind velocity of 14.1 m/s within an altitude range below 2000 m at 9:00 at Kagoshima, approximately 45 km from Shinmoedake [49]. Therefore, the SO_2 column amount peaks can be interpreted as degassing from Shinmoedake

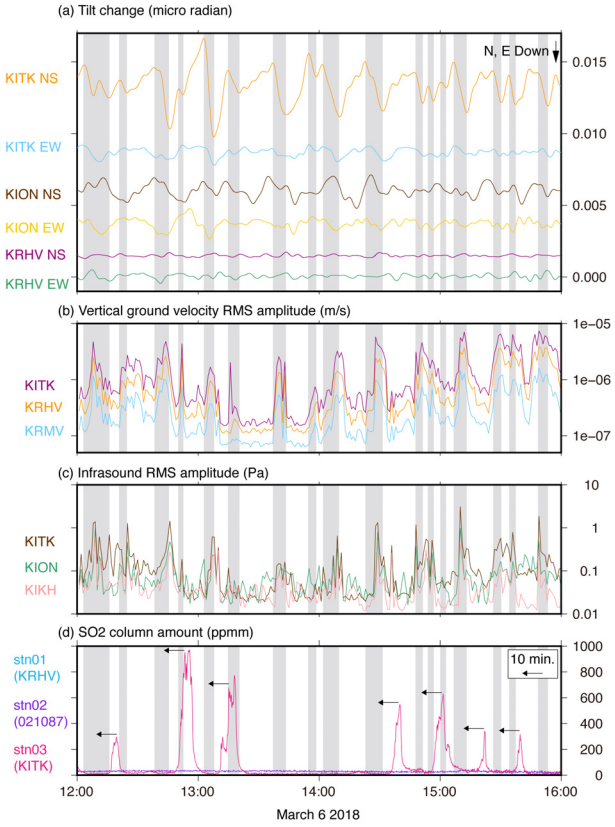

Fig. 12. Time series of a dataset for 4 h from 12:00 on March 6. The periods when the tilt records at KITK showed southward uplift are highlighted in gray. (a) Filtered (5.0×10^{-4}–4.0×10^{-3} Hz) tilt records with an acausal filter. (b) RMS amplitude of the 1-min average of vertical ground veclocity. (c) RMS amplitude of the 1-min average of infrasound records. (d) Sulfer dioxide column amount with time.

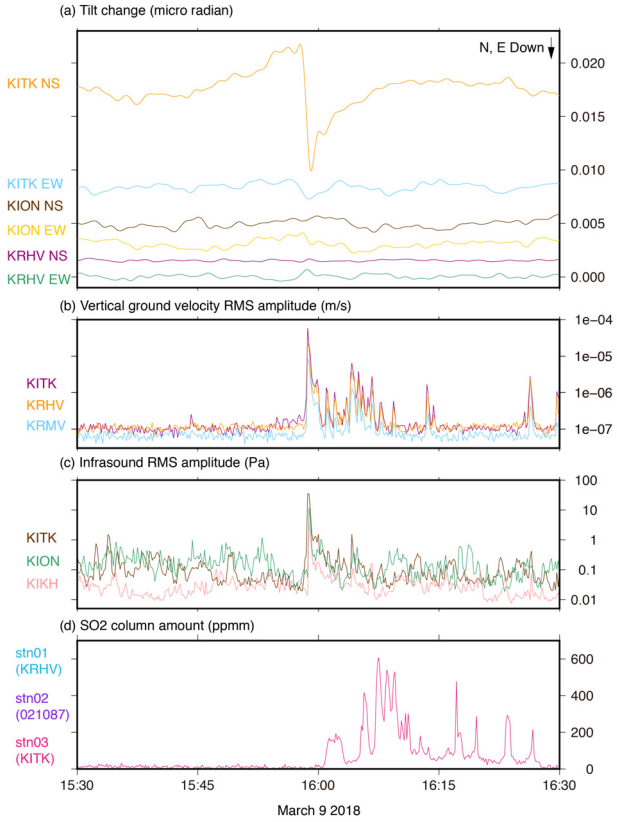

Fig. 13. Time series of dataset accompanying the Vulcanian eruption on March 9, 2018. (a) Filtered (5.0×10^{-4}–0.01 Hz) tilt records with an acausal filter. (b) RMS amplitude of the 1-min average of vertical ground veclocity. (c) The RMS amplitude of the 1-min average of infrasound records. (d) Sulfer dioxide column amount change with time.

associated with each RMS amplitudes increase event. The coincident changes in seismic and infrasound RMS amplitudes, inflation-deflation tilt events at KITK, and the swarm of LF events continued for 41 h from March 6 (at approximately 07:00), which is almost the same period of ground deformation in the tilt data (**Fig. 9(a)**). This period is also when the lava extruding at an average rate of 72 m^3/s as inferred by Synthetic Aperture Radar (SAR) data [50]. Hence, these signals are related to the lava extrusion. **Fig. 10(e)** shows a video still of Shinmoedake at 15:00 on March 9. The image captures the new lava dome formed in the crater.

The number of LF events again increases on March 9 (**Fig. 9(c)**). **Figure 13** shows the 1-h time series of filtered (5.0×10^{-4}–0.01 Hz) tilt records (**Fig. 13(a)**), 1-min RMS of seismic and infrasound amplitudes (**Figs. 13(b)** and **(c)**), and SO_2 column amount (**Fig. 13(d)**) from 15:30 on March 9. The KITK tilt shows a northward uplift from 15:45. At 15:58, the polarity of the tilt suddenly changes to southward uplift, and returns to northward uplift after 2 min. A second change in the tilt polarity was associated with a sudden increase in both seismic (**Fig. 13(b)**) and infrasound (**Fig. 13(c)**) amplitudes. After the sudden release of seismic and infrasound signals, the SO_2 column amount gradually increased, suggesting that emitted volcanic gas passed over the station. A series of signals shown in **Fig. 13** was associated with the first Vulcanian eruption during the 2018 eruption at Shinmoedake. Following this first event, Shinmoedake had intermittent Vulcanian eruptions until May 22, 2018 [51]. These Vulcanian eruptions were recorded in **Fig. 9** as a simultaneous pulse-like increase in seismic and infrasound amplitude, and occasionally in SO_2 column amount.

4. Discussion

4.1. Long-Term Volcanic Activity (2011–2018)

Our dataset shows that the GNSS data recorded the continuous extension of the length of the horizontal baseline of each station pair following the 2011 eruption. The extension accelerated following the 2017 eruptions and changed to a contraction during lava extrusion of the 2018 eruption. After the lava extrusion, all lengths showed extension again. The cycle of pre-eruptive changes in extensional baseline length, sudden syn-eruptive contraction, and post-eruptive re-extension is nearly the same as that documented for the 2011 eruption (**Fig. 2(a)**). Although

detailed modeling of the deformation will be necessary for further discussions, we posit that the GNSS data has successfully captured the magma intrusion into or pressure build-up in the magma chamber that drove the 2017 and the 2018 eruptions. The continuous return to extension/uplift following each of these eruptions suggests that there is continued magma recharge in the system and that future eruptions are still probable.

Another implication for long-term volcanic activity from our dataset can be taken from the seismicity data. Important increases in seismicity precede nearly all eruptions world-wide [10–13], and the 2017 and the 2018 eruptions. In the case of the 2017 and 2018 eruptions at Shinmoedake, our dataset also showed important increases in seismicity (both HF and LF events) starting during 2016 (**Fig. 2**). However, although some seismic swarms of HF events occurred during the inter-eruptive period from 2011 to 2018, not all events were accompanied by eruptions and the precise threshold for seismic increases at Shinmoedake that lead to the eruptions needs to be determined from many eruptive cycles, similar to that calculated in White and McCausland [12]. White and McCausland [12] concluded that the cumulative magnitude of distal and proximal events can be a useful index for forecasting upcoming eruptions at volcanoes without eruptions over at least 25 years. Following this method, we plotted the time history of the magnitude of distal and proximal events in **Figs. 4** and **6**, respectively. However, because most events in our dataset have a magnitude less than 0, the cumulative values shown in **Figs. 4** and **6** do not represent the entire observed seismicity. This is clearly recognized for the proximal HF and LF events, when comparing the event number in **Figs. 2** and **5** and the cumulative magnitude **Figs. 4** and **6**. Because we focused on the period following the 2011 eruptions, the difference in conditions among the volcanoes is one of the possible factors for the discrepancy, as well as the quality of earthquake catalog. An increase in seismicity in the Kirishima volcano complex and around Shinmoedake has been reported since the 1960s [52]. Analyses of focal mechanisms suggest that the seismicity is induced by an extensional stress field in a northwest (NW) to southeast (SE) direction [53]. In addition, our seismic data includes events related to activity at Iwoyama, at least since late 2015 [23]. During the period between 2012 and 2015, the eastern Kirishima area had a relatively high HF seismicity at 10 km depth (**Fig. 3**). Kagiyama [54] reported an intense seismicity in this area during the 1980s and 1990s and proposed a conceptual model for the activity considering a NW-SE extensional stress field over the Kirishima volcano complex, rather than a stress change from a magmatic process. In the model of White and McCausland [12], this seismicity would be considered to be distal VT seismicity related to the Kirishima volcanic complex. This eastern seismicity decreased beginning in 2016, and remained at a low rate during the 2018 eruptions (**Fig. 5**). The relationship between this seismicity and the eruption pattern of Shinmoedake is worth further study.

From **Figs. 2–4**, it is apparent that DLP events occur at a constant rate regardless of the activity of Shinmoedake. The epicenters are focused on east-south of Shinmoedake. This is a remarkable contrast to the magma chamber driving eruptions at Shinmoedake is on the other side of the Kirishima volcano complex (e.g., [32]). Deep low frequency events beneath active volcanoes have been reported in worldwide (e.g., [55–58]) and several conceptual models of their source dynamics have been proposed (e.g., [59–61]). Accumulating more data may enable to the discuss of the relationship between the DLF events and eruption activity within a broad time window.

4.2. Precursors (Days to Week Range)

Figures 5 and **6** show that the number of proximal HF and LF events begins to increase on October 3, 8 days before the onset of the 2017 eruption.

In the case of the 2017 eruption, the tilt-change event preceded the onset of the ash emissions by 38 h (**Fig. 5**). Although a detailed analysis is necessary to discuss the source characteristic of the event, the maximum tilt change at KITK in our dataset suggests that the pressure source was beneath Shinmoedake, rather than the magma chamber inferred on the west side of the Kirishima volcano complex (e.g., [32]). Ichihara and Matsumoto [62] also reported a tilt-change event approximately 30 min prior to the first phreatic event during the 2011 eruption. Similar tilt events preceding volcanic eruptions have been reported worldwide [63–65]. The proximal seismicity and tilt events may represent the process leading to upcoming eruptions, such as the interaction between underground water and ascending magma (e.g., [66]). Instead, significant precursory changes in the seismicity tilt record were not recognized prior to the 2018 eruption in the time scale of several weeks (**Figs. 5**, **6**, and **9**). The difference in the precursor changes of both eruptions in the observational data can reflect the shallow conduit system and is worth examining in detail.

Both the 2017 and 2018 eruptions share increases in the RMS amplitudes and relative amplitudes at KITK with respect to other more distant stations. This change was recognized 40 h prior to the onset of the 2017 eruption (**Fig. 7**), and 3 h in the case of the 2018 eruption (**Fig. 9**). Because the event numbers for proximal HF and LF events did not increased significantly with the relative RMS amplitude, this change was likely because of the start of a continuous tremor at the volcano. A continuous volcanic tremor from beneath Shinmoedake was reported during the 2011 eruption [62, 67, 68]. Hence, the occurrence of continuous tremor may be an important precursor for upcoming eruptions. Although not shown here, the location of the tremor has been shown to provide valuable with which to evaluate volcanic activity (e.g., [69–72]).

Volcanic gas data can also provide precursory signals prior to volcanic eruptions (e.g., [73]). Because our SO_2 data reflect the total column amount above each station, the detection ability highly depends on atmospheric conditions. Although not shown here, our data occasionally

recorded not only gases from Shinmoedake, but also from Sakurajima, an active volcano approximately 45 km south of Shinmoedake, depending on the atmospheric condition. Hence, detailed examinations are needed to determine the precursory signals from column data.

The video stills in **Figs. 8(a)** and **(b)** show the considerable increase in fumaroles height prior to the 2017 eruption. This change can reflect the process leading to the onset of the 2017 eruption, although fumaroles behavior could potentially be affected by atmospheric conditions and local topography (e.g., [74]).

Our infrasound data could not resolve any considerable signals prior to the onset of the 2017 and 2018 eruptions. However, if the signal-to-noise ratio is sufficient, instruments may record acoustic signals associated with some increases in surface activity, such as fumaroles [75].

4.3. Syn-Eruptive Signals

As our dataset has shown, video, infrasound, and SO_2 gas data are powerful tools with which to evaluate the nature of eruptive activity. Visual image data are the most straightforward for confirmation and understanding eruption behavior, although the quality of data in visual spectrum depends on the visibility at the vent area.

Infrasound observation is effective in detecting and quantifying the degassing phenomena (e.g., [76, 77]). However, wind and artificial noises can inhibit recognition of the signal from volcanic eruptions from noise in an infrasound record (**Figs. 7(e)** and **9(e)**). Examining cross-correlation or coherence between an array of infrasound stations or co-located infrasound and vertical seismograms from co-located sites are effective means to distinguish eruptive signals from noise at Shinmoedake in the future [78, 79].

Figure 12(d) suggests that not all degassing signals recorded in seismic and infrasound RMS amplitude correspond to those of the SO_2 column data. These inconsistences may be because some eruption plumes and volcanic gas were emitted passively and therefore not detected by the sensors. Improving detection ability and station coverage remains challenging for continuous SO_2 measurements. In addition, measuring other gas species would improve the connections among seismic, infrasound, geodetic and gas measurements [80].

During three sub-Plinian eruptions and lava extrusion during the 2011 eruption of Shinmoedake, geodetic observations captured syn-eruptive magma chamber contraction [32]. The deflation of the magma chamber was well-correlated to the magma discharge rate at the surface [81]. The tilt and the GNSS data of ground deformation during the lava extrusion of the 2018 eruption is explained by the same pressure source as that modeled for the 2011 eruption [82]. Because geodetic data are typically transmitted to observatories in real-time, the data can be useful to evaluate the magma discharge rate of ongoing eruptions.

4.4. Implications from Other Volcanoes

Figure 12 shows the data accompanying periodic degassing and the corresponding inflation-deflation tilt cycles of the volcanic edifice during the 2018 lava extrusion. Such periodic tilt changes and excitation of tremors were also observed accompanying the lava dome effusion of the 2011 eruption of Shinmoedake [83]. At Santiaguito, similar periodic degassing and relating inflation-deflation cycle were reported accompanying lava dome formation [3, 84]. Thus, periodic degassing and inflation-deflation cycles may be a fundamental process of effusive eruptions and a more extensive review of cases is suggested. If this is true, measurement of cyclic degassing may be a means to detect lava effusion and lava dome formation from continuous data in poor visibility conditions. Because lava dome collapses cause pyroclastic density currents [85, 86], understanding and detecting lava dome growth in places where the dome growth can become unstable is an important part of hazard mitigation in volcano monitoring.

Vulcanian eruptions are equally important to hazard mitigation (**Fig. 13**). Inflation prior to Vulcanian eruptions was reported during the 2011 eruption [21, 83], while reversals of ground deformation following inflation is also reported at other volcanoes [63]. With such diversity, further studies are necessary to examine the dynamics behind the deformation signals accompanying Vulcanian eruptions at Shinmoedake and other volcanoes. This is necessary to contextualize the similarities and differences in the data and therefore the underlying processes. Furthermore, information regarding volcanic activity and disasters and the society response to them are important parameters to consider in addition to monitoring data for the most effective utilization of a multiparameter volcano dataset.

5. Summary

We have examined the multiparameter observations at Shinmoedake volcano between 2010 and 2018 and compared them to the volcanic activity chronology. The GNSS data successfully recorded ground extension that suggests consistent pressure build-up or magma intrusion in the magma storage region since 2014. Precursors to the 2017 and 2018 eruptions were captured as the number of HF and LF events of volcanic earthquakes from 2016, and the RMS seismic amplitude approximately 3–40 h prior to the onset of the eruption. However, it seems that the number of HF events does not always directly relate to the volcanic activity. Continuous ash emissions and lava effusion during the 2017 and 2018 eruptions were recorded throughout LF event seismicity, video images, the RMS seismic and infrasound amplitude, SO_2 column amount, and tilt data. Some aspects of observational data share similar characteristics of those of lava effusion and Vulcanian eruptions at other volcanoes. We demonstrate that our multiparameter dataset covers a broad spatiotemporal scale for volcanic activity: from magma intrusion for

several years to transient degassing at the vent. Such a coverage of volcanic phenomena will contribute to construct a comprehensive model to explain the physics behind volcanic activity. However, defining a quantitative threshold between the background and an active state for practical volcano monitoring remains a challenge. Further studies and continuous observation are needed to quantify the overall volcanic activity within a broader time scale. By understanding what are the important changes in monitoring data prior to and during volcanic activity at Shinmoedake, we can seek to adopt this method of multiparameter volcanic databases to evaluate ongoing eruptions and unrest at Shinmoedake and volcanoes worldwide.

Acknowledgements

We acknowledge the JMA for providing observation data, the GSI for providing observation data and digital elevation map of the Kirishima area. Many thanks to the staff of Volcano Disaster Resilience Research Division of the NIED for supporting the operation of the V-net. TY is grateful to Dr. Higashi Uchida at Kagoshima Local Meteorological Observatory, JMA, for providing information regarding the instrumentation of the network of the JMA, and Dr. Ryohei Kawaguchi at the Meteorological Research Institute, JMA, for providing video image data. Critical reviews and comments by anonymous reviewers significantly improved the manuscript. The present study was partly supported by the Ministry of Education, Culture, Sports, Science, and Technology (MEXT) of Japan, under its Integrated Program for Next Generation Volcano Research and Human Resource Development.

References:

[1] H. Aoyama and H. Nakamichi, "Eruption Process Inferred from Multi-parameter Geophysical Observations," Bull. Volcanol. Soc. Japan, Vol.61, pp. 119-154, 2016.

[2] M. P. Dalton, G. P. Waite, I. M. Watson, and P. A. Nadeau, "Multiparameter quantification of gas release during weak Strombolian eruptions at Pacaya Volcano, Guatemala," Geophys. Res. Lett., Vol.37, L09303, 2010.

[3] J. B. Johnson, J. J. Lyons, B. J. Andrew, and J. M. Lees, "Explosive dome eruptions modulated by periodic gas-driven inflation," Geophys. Res. Lett., Vol.41, pp. 6689-6697, 2014.

[4] R. Kazahaya, Y. Maeda, T. Mori, H. Shinohara, and M, Takeo, "Changes to the volcanic outgassing mechanism and very-long-period seismicity from 2007 to 2011 at Mt. Asama, Japan," Earth Planet. Sci. Lett., Vol.418, pp. 1-10, 2015.

[5] D. Fee, P. Izbekov, K. Kim, A. Yokoo, T, Lopez, F. Prata, R. Kazahaya, H. Nakamichi, and M. Iguchi, "Eruption mass estimation using infrasound waveform inversion and ash gas measurements: Evaluation at Sakurajima Volcano, Japan," Earth Planet. Sci. Lett., Vol.480, pp. 42-52, 2017.

[6] C. G. Newhall, F. Costa, A. Ratdomopurbo, D. Y. Venezky, C. Widiwijayanti, N. T. Z. Win, K. Tan, and E. Fajiculay, "WOVOdat – An online, growing library of worldwide volcanic unrest," J. Volcanol. Geotherm. Res., Vol.345, pp. 184-199, 2017.

[7] H. Ueda, T. Yamada, T, Miwa, M. Nagai, and T. Matsuzwa, "Development of a Data Sharing System for Japan Volcanological Data Network," J. Disaster Res., Vol.14, No.4, pp. 571-579, 2019.

[8] T. E. Sheldrake, R. S. J. Sparks, K. V. Cashman, G. Wadge, and W. P. Aspinall, "Similarities and differences in the historical records of lava dome-building volcanoes: Implications for understanding magmatic processes and eruption forecasting," Earth Sci. Rev., Vol.160, pp. 240-263, 2016.

[9] T. Minakami, "Fundamental research for predicting volcanic eruptions: Part 1," Bull. Earth Res. Inst., Vol.38, pp. 497-544, 1960.

[10] S. R. McNutt, "Seismic monitoring and eruption forecasting of volcanoes: a review of the state-of-the-art and case histories," R. Scarpa and R. I. Tilling (Eds.), Monitoring and Mitigation of Volcanic Hazards, pp. 99-146, Springer-Verlag, Berlin, 1994.

[11] T. Nishimura and M. Iguchi, "Volcanic Earthquakes and Tremor in Japan," Kyoto University Press, Kyoto, 2011.

[12] R. White and W. McCausland, "Volcano-tectonic earthquake: A new tool for estimating intrusive volumes and forecasting eruptions," J. Volcanol. Geotherm. Res., Vol.309, pp. 139-155, 2016.

[13] W. A. McCausland, H. Gunawan, R. A. White, N. Indrastuti, C. Patria, Y. Suparman, A. Putra, H. Triastuty, and M. Hendrasto, "Using a process-based model of pre-eruptive seismic patterns to forecast evolving eruptive styles at Sinabung Volcano, Indonesia," J. Volcanol. Geotherm. Res., doi: 10.1016/j.jvolgeores.2017.04.004, 2017.

[14] R. A. White and W. A. McCausland, "A process-based model of pre-eruption seismicity patterns and its use for eruption forecasting at dormant stratovolcanoes," J. Volcanol. Geotherm. Res., doi: 10.1016/j.jvolgeores.2019.03.004, 2019.

[15] D. Dzurisin, "A comprehensive approach to monitoring volcano deformation as a window on the eruption cycle," Rev. Geophys., Vol.41, Issue 1, doi: 10.1029/2001RG000107, 2003.

[16] L. Feng and A. V. Newman, "Constraints on continued episodic inflation at Long Valley Caldera, based on seismic and geodetic observations," J. Geophys. Res., Vol.114, doi: 10.1029/2008JB006240, 2009.

[17] M. Iguchi, "Magma movement from the deep to shallow Sakurajima volcano revealed by geophysical observations," Bull. Volcanol. Soc. Jpn., Vol.58, pp. 1-18, 2013.

[18] S. Nagaoka and M. Okuno, "Tephrochronology and eruptive history of Kirishima volcano in southern Japan," Quatern. Int., Vol.246, pp. 260-269, 2011.

[19] R. Imura and T. Kobayashi, "Eruptions of Shinmoedake Volcano, Kirishima Volcano Group, in the Last 300 Years," Bull. Volcanol. Soc. Jpn., Vol.36, pp. 135-148, 1991.

[20] S. Nakada, M. Nagai, T. Kaneko, Y. Suzuki, and F. Maeno, "The outline of the 2011 eruption at Shinmoe-dake (Kirishima), Japan," Earth Planets Space, Vol.65, pp. 475-488, 2013.

[21] K. Kato and H. Yamasato, "The 2011 eruptive activity of Shinmoedake volcano, Kirishimayama, Kyushu, Japan – Overview of activity and Volcanic Alert Level of the Japan Meteorological Agency –," Earth Planets Space, Vol.65, pp. 489-504, 2013.

[22] M. Tsutsui, K. Tomita, and T. Kobayashi, "Fumarolic Activity since December 2003 and Volcanic Activity during the Meiji and Taisho Eras (1880–1923) of Ohachi Volcano, Kirishima Volcano Group, Southern Kyushu, Japan," Bull. Volcanol. Soc. Jpn., Vol.50, pp. 475-489, 2005.

[23] Japan Meteorological Agency, "Kirishimayama," Paper presented at 141th meeting of Coordinating Committee for Prediction of Volcanic Eruptions, Japan Meteorological Agency, Tokyo, 2018, https://www.data.jma.go.jp/svd/vois/data/tokyo/STOCK/kaisetsu/CCPVE/CCPVE08.html (in Japanese) [accessed December 18, 2018]

[24] Y. Tajima, Y. Matsuo, A. Matsuoka, T. Shoji, H. Itoh, and T. Kobayashi, "Eruptive history for the last 10,000 years of Ebinokogen area in Kirishima volcano group, southern Kyushu," Programme and Abstracts, The Volcanological Society of Japan, p. 40, 2008.

[25] T. Tanada, H. Ueda, M. Nagai, and M. Ukawa, "NIED's V-net, the Fundamental Volcano Observation Network in Japan," J. Disaster Res., Vol.12, No.5, pp. 926-931, 2017.

[26] Japan Meteorological Agency, "Volcano observation at Kirishima Volcano," 2018, https://www.data.jma.go.jp/svd/vois/data/fukuoka/505_Kirishimayama/505_Obs_points.html (in Japanese) [accessed December 18, 2018]

[27] T. Sagiya, "A decade of GEONET: 1994–2003 – The continuous GPS observation in Japan and its impact on earthquake studies –," Earth Planets Space, Vol.56, pp. xxix-xli, 2004.

[28] B. Galle. C. Oppenheimer, A. Geyer, A. J. S. McGonigle, M. Edmonds, and L. Horrockes, "A miniaturised ultraviolet spectrometer for remote sensing of SO_2 fluxes: a new tool for volcano surveillance," J. Volcanol. Getherm. Res., Vol.119, pp. 241-254, 2002.

[29] T. Mori, J. Hirabayashi, K. Kazahaya, T. Mori, M. Ohwada, M. Miyashita, H. Iino, and Y. Nakahori, "A Compact Ultraviolet Spectrometer System (COMPUSS) for Monitoring Volcanic SO, Emission: Validation and Preliminary Observation," Bull. Volcano. Soc. Jpn., Vol.52, pp. 105-112, 2007.

[30] T. Mori and K. Karto, "Sulfur dioxide emissions during the 2011 eruption of Shinmoedake volcano, Japan," Earth Planets Space, Vol.65, pp. 573-580, 2013.

[31] T. Mori, T. Hashimoto, A. Terada, M. Yoshimoto, R. Kazahaya, H. Shinohara, and R. Tanaka, "Volcanic plume measurements using a UAV for the 2014 Mt. Ontake eruption," Earth Planets Space, Vol.68, doi: 10.1186/s40623-016-0418-0, 2016.

[32] H. Ueda, T. Kozono, R. Fujita, Y. Kohno, M. Nagai, Y. Miyagi, and T. Tanada, "Crustal deformation associated with the 2011 Shinmoedake eruption as observed by tiltmeters and GPS," Earth Planets Space, Vol.65, pp. 517-525, 2013.

[33] Y. Miyagi, T. Ozawa, and K. Kohno, "Crustal deformation associated with the 2011 Eruption of Shinmoe-dake in Kirishima Volcano Group, Southwestern Japan, detected by DInSAR and GPS measurements," Bull. Volcanol. Soc. Jpn., Vol.54, pp. 341-351, 2013 (in Japanese with English abstract).

[34] S. Nakao, Y. Morita. H. Yakiwara, J. Oikawa, H. Ueda, H. Takahashi, Y. Ohta, T. Matsushima, and M. Iguchi, "Volume change of the magma reservoir relating to the 2011 Kirishima Shinmoe-dake eruption – Charging, discharging and recharging process inferred from GPS measurements," Earth Planets Space, Vol.65, pp. 505-515, 2013.

[35] Y. Miyagi, T. Ozawa, T. Kozono, and M. Shimada, "Long-term lava extrusion after the 2011 Shinmoe-dake eruption detected by DInSAR observations," Geophys. Res. Lett., Vol.41, pp. 5855-5860, 2014.

[36] Y. Himematsu and M. Furuya, "Fault source model for the 2016 Kumamoto earthquake sequence based on ALOS-2/PALSAR-2 pixel-offset data: evidence for dynamic slip partitioning," Earth Plants Space, Vol.68, doi: 10.1186/s40623-016-0545-7, 2016.

[37] K. Heki, S. Miyazaki, and H. Tsuji, "Silent fault slip following an interplate thrust earthquake at the Japan Trench," Nature, Vol.386, pp. 595-598, 1997.

[38] Japan Meteorological Agency, "Kirishimayama," paper presented at 140th meeting of Coordinating Committee for Prediction of Volcanic Eruptions, Japan Meteorological Agency, Tokyo, 2018, https://www.data.jma.go.jp/svd/vois/data/tokyo/STOCK/kaisetsu/CCPVE/CCPVE08.html (in Japanese) [accessed December 18, 2018]

[39] Geospatial Information Authority of Japan, "Kirishimayama," Paper presented at 141th meeting of Coordinating Committee for Prediction of Volcanic Eruptions, Japan Meteorological Agency, Tokyo, 2018, https://www.data.jma.go.jp/svd/vois/data/tokyo/STOCK/kaisetsu/CCPVE/CCPVE08.html (in Japanese) [accessed December 18, 2018]

[40] National Institute for Earth Science and Disaster Resilience, "Kirishimayama," Report of Coordinating Committee for Prediction of Volcanic Eruption, No.117, Japan Meteorological Agency, Tokyo, 2015 (in Japanese).

[41] T. Horikoshi, J. Takayama, K. Takeshita, K. Goko, and H. Yoshizawa, "An analysis of the geothermal structure of the Ogiri geothermal field based on the surveys and operational data of the Ogiri Power Station after its commencement," J. Soc. Resource Geology, Vol.55, pp. 25-38, 2005.

[42] M. Cardiff, D. D. Lim, J. R. Patterson, J. Akerley, P. Spielman, J. Lopeman, P. Walsh, A. Singh, W. Foxall, H. F. Wang, N. E. Lord, C. H. Thunder, D. Fratta, R. J. Mellors, N. C. Davatzes, and K. L. Feigl, "Geothermal production and reproduced seismicity: Correlation and proposed mechanism," E. Plant Sci. Lett., Vol.482, pp. 470-477, 2018.

[43] D. Juncu, Th. Ánadóttir, H. Geirsson, G. B. Gudmundsson, B. Lund, G. Gunnarsson, A. Hooper, S. Hreinsdóttir, and K. Michalczewska, "Injection-induced surface deformation and seismicity at the Hellisheidi geothermal field, Iceland," J. Volcanol. Geotherm. Res., doi: 10.1016/j.jvolgeores.2018.03.019, 2018.

[44] D. C. Agnew, "Strainmeters and Tiltmeters," Rev. Geophys., Vol.24, pp. 579-624, 1986.

[45] Y. Aoki, "Recent Progress of Volcano Deformation Studies," Bull. Vol. Soc. Jpn., Vol.61, pp. 311-344, 2016.

[46] G. D. Moro and M. Zabro, "Subsurface deformations induced by rainfall and atmospheric pressure: tilt/strain measurements in the NE-Italy seismic area," Earth Planet. Sci. Lett., Vol.164, pp. 193-203, 1998.

[47] Y. Tamura, T. Sato, M. Ooe, and M. Ishiguro, "A procedure for tidal analysis with a Bayesian information criterion," Geophys. J. Int., Vol.104, pp. 507-516, 1991.

[48] Japan Meteorological Agency, "Meteorological data archive," 2018, https://www.data.jma.go.jp/obd/stats/etrn/index.php (in Japanese) [accessed June 26, 2019]

[49] University of Wyoming, "Sounding data of upper air data," 2018, http://weather.uwyo.edu/upperair/sounding.html [accessed June 26, 2019]

[50] National Institute for Earth Science and Disaster Resilience, "Kirishimayama," Paper presented at 141th meeting of Coordinating Committee for Prediction of Volcanic Eruptions, Japan Meteorological Agency, Tokyo, 2018, https://www.data.jma.go.jp/svd/vois/data/tokyo/STOCK/kaisetsu/CCPVE/CCPVE08.html (in Japanese) [accessed December 18, 2018]

[51] Japan Meteorological Agency, "Eruption list of Shinmoedake volcano in 2018," Japan Meteorological Agency, Kagoshima, 2018, http://www.jma-net.go.jp/kagoshima/ (in Japanese) [accessed December 18, 2018]

[52] T. Minakami, M. Hagiwara, M. Yamaguchi, E. Koyama, and K. Hirai, "The Ebino earthquake Swarm and the Seismic Activity in the Kirishima Volcanoes, in 1968-1969, Part 4: Shifts of Seismic Activity from the Kakuto Caldera to Shinmoe-dake, Naka-dake and Takatiho-mine," Bull. Earthq. Res. Inst., Vol.48, pp. 205-233, 1970.

[53] Y. Ida, M. Yamaguchi, and F. Masutani, "Recent Seismicity and Stress Field in Kirishima Volcnao," J. Seism. Soc. Jpn., Vol.103, pp. 479-487, 1994 (in Japanese with English abstract).

[54] T. Kagiyama, "Kirishima Volcanoes – Multi active volcanic group generated in a slightly tensile stress field," J. Tokyo Geogr. Soc., Vol.103, pp. 479-487, 1994.

[55] K. Aki and R. Koyanagi, "Deep Volcanic Tremor and Magma Ascent Mechanism Under Kulauea, Hawaii," J. Geophys. Res., Vol.86, pp. 7095-7109, 1981.

[56] M. Ukawa and M. Ohtake, "A monochromatic earthquake suggesting deep!-seated magmatic activity beneath the Izu!-Ooshima Volcano, Japan," J. Geophys. Res., Vol.92, pp. 12649-12663, 1987.

[57] J. A. Power, S. D. Stihle, R. A. White, and S. C. Moran, "Observations of deep long-period (DLP) seismic events beneath Aleutian arc volcanoes; 1989–2002," J. Volcanol. Geotherm. Res., Vol.138, pp. 243-266, 2004.

[58] M. Ukawa, "Deep Low-frequency earthquake swarm in the mid crust beneath Mount Fuji (Japan) in 2000 and 2001," Bull, Volcanol., Vol.68, pp. 67-56, 2005.

[59] H. Nakamichi, M. Ukawa, and S. Sakai, "Precise hypocenter locations of midcrustal low-frequency earthquakes beneath Mt. Fuji, Japan," Earth Planets Place, Vol.56, pp. e37-e40, 2004.

[60] N. Aso and V. C. Tsai, "Cooling magma model for deep volcanic long-period earthquakes," J. Geophys. Res., Vol.119, pp. 8442-8456, 2014.

[61] N. M. Shapiro, D. V. Droznin, S. Ya. Droznina, S. L. Senyukov, A. A. Gusev, and E. I. Gordeev, "Deep and shallow long-period volcanic seismicity linked by fluid-pressure transfer," Nat. Geosci., Vol.10., pp. 442-445, 2017.

[62] M. Ichihara and S. Matsumoto, "Relative Source Locations of Continuous Tremor Before and After Subplinian Events at Shinmoe-dake, in 2011," Geophys. Res. Lett., Vol.44, 10871-10877, 2017.

[63] M. Iguchi, H. Yakiwara, T. Tameguri, M. Hendrasto, and J. Hirabayashi, "Mechanism of explosive eruption revealed by geophysical observations at the Sakurajima, Suwanosejima and Semeru volcanoes," J. Volcanol. Geotherm. Res., Vol.178, pp. 1-9, 2008.

[64] T. Nishimura, M. Iguchi, R. Kawaguchi, Surono, M. Hendrasto, and U. Rosadi, "Inflation prior to Vulcanian eruptions and gas bursts detected by tilt observations at Semeru Volcano, Indonesia," Bull. Volcanol., Vol.74, pp. 903-911, 2012.

[65] H. Aoyama and H. Oshima, "Precursory tilt changes of small phreatic eruptions of Meakan-dake volcano, Hokkaido, Japan, in November 2008," Earth Planets Space, 67:119, 2015.

[66] E. Fujita, "Banded tremor at Miyakejima volcano, Japan: Implication for two-phase flow instability," J. Geophys. Res., Vol.113, doi: 10.1029/2006JB004829, 2008.

[67] S. Matsumoto, H. Shimizu, T. Matsushima, K. Uehira, Y. Yamashita, M. Nakamoto, M. Miyazaki, and H. Chikura, "Short-term spatial change in a volcanic tremor source during the 2011 Kirishima eruption," Earth Planets Space, Vol.65, pp. 323-329, 2013.

[68] H. Nakamichi, Y. Yamanaka, T. Terakawa, S. Horikawa, T. Okuda, and F. Yamazaki, "Continuous long-term array analysis of seismic records observed during the 2011 Shinmoedake eruption activity of Kirishima volcano, Southwest Japan," Earth Planets Space, Vol.65, pp. 551-562, 2013.

[69] J. Battaglia and K. Aki, "Location of seismic events and eruptive fissures on the Piton de la Fournaise volcano using seismic amplitudes," J. Geophys. Res., Vol.108, doi: 10.1029/2002JB002193, 2003.

[70] M. Ogiso and K. Yomogida, "Migration of tremor locations before the 2008 eruption of Meakandake Volcano, Hokkaido, Japan," J. Volcanol. Geotherm. Res., Vol.217-218, pp. 8-20, 2012.

[71] H. Kumagai, P. Mothes, M. Ruiz, and Y. Maeda, "An approach to source characterization of tremor signals associated with eruptions and lahars," Earth Planets Space, Vol.67, doi: 10.1186/s40623-015-0349-1, 2015.

[72] A. Kurokawa, M. Takeo, and K. Kurita, "Two types of volcanic tremor changed with eruption style during 1986 Izu-Oshima eruption," J. Geophys. Res., Vol.121, pp. 2727-2736, 2016.

[73] J. M. de Moor, A. Aiuppa, J. Pacheco, G. Avard, C. Kern, M. Liuzzo, M. Martínez, G. Giudice, and T.P. Fischer, "Short-period volcanic gas precursors to phreatic eruptions: insight from Poás Volcano, Costa Rica," Earth Planet. Sci. Lett., Vol.442, pp. 218-227, 2016.

[74] A. Terada, "Evaluation of the Heat Discharge Rates from Vent "A" at Tarumae Volcano, Japan: Note on the Plume Rise Assumption," Geophysical Bulletin of Hokkaido University, No.67, pp. 327-335, 2004.

[75] K. McKee, D. Fee, A. Yokoo, R. S. Matoza, and K. Kim, "Analysis of gas jetting and fumarole acoustics at Aso Volcano, Japan," J. Volcanol. Geotherm. Res., Vol.340, pp. 16-29, 2017.
[76] J. B. Johnson and M. Ripepe, "Volcano infrasound: A review," J. Volcanol. Geothrm. Res., Vol.206, pp. 61-69, 2011.
[77] D. Fee and R. S. Matoza, "An overview of volcano infrasound: From hawaiian to plinian, local to global," J. Volcanol. Geotherm. Res., Vol.249, pp. 123-139, 2013.
[78] M. Ichihara, M. Takeo, A. Yokoo, J. Oikawa, and T. Ohminato, "Monitoring volcanic activity using correlation patterns between infrasound and ground motion," Geophys. Res. Lett., Vol.34, L04304, 2012.
[79] R. S. Matoza and D. Fee, "Infrasonic component of volcano seismic eruption tremor," Geophys. Res. Lett., Vol.41, pp. 1964-1970, 2014.
[80] E. Padrón, N. M. Pérez, P. A. Hernández, H. Sumino, G. V. Melián, J. Barrancos, D. Nolasco, G. Padilla, S. Dionis, F. Rodríguez, Í. Hernández, D. Calvo, M. D. Peraza, and K. Nagao, "Diffusive helium emissions as a precursory sign of volcanic unrest," Geology, Vol.41 pp. 539-542, 2013.
[81] T. Kozono, H. Ueda, T. Shimbori, and K. Fukui, "Correlation between magma chamber deflation and eruption cloud height during the 2011 Shinmoe-dake eruptions," Earth Planets Space, Vol.66, doi: 10.1186/s40623-014-0139-1, 2014.
[82] H. Ueda, "Mechanism of the Shinmoe-dake eruptions in 2011 and 2018 inferred from crustal deformation data," Programme and Abstracts, The Volcanological Society of Japan, 2018.
[83] M. Takeo, Y. Maehara, M. Ichihara, T. Ohminato, R. Kamata, and J. Oikawa, "Ground deformation cycles in a magma-effusive stage, and sub-Plinian and Vulcanian eruptions at Kirishima volcanoes, Japan," J. Geophys. Res., Vol.118, pp. 4758-4773, 2013.
[84] A. S. P. Holland, I. M. Watson, J. C. Phillips, L. Caricchi, and M. P. Dalton, "Degassing processes during lava dome growth: Insight from Santiaguito lava dome, Guatemala," J. Volcanol. Geotherm., Res., Vol.202. pp. 153-166, 2011.
[85] T. Fujii and S. Nakada, "The 15 September 1991 pyroclastic flows at Unzen Volcano (Japan): a flow model for associated ash-cloud surges," J. Volcanol. Geotherm. Res., Vol.89. pp. 159-172, 1999.
[86] S. Nakada, A. Zaennudin, M. Yoshimoto, F. Maeno, Y. Suzuki, N. Hokanishi, H. Sasaki, M. Iguchi, T. Ohkura, H. Gunawan, and H. Triastuty, "Growth process of the lava dome/flow complex at Sinabung Volcano during 2013–2016," J. Volcanol. Geotherm. Res., doi: 10.1016/j.jvolgeores.2017.06.012, 2017.

Name:
Taishi Yamada

Affiliation:
National Research Institute for Earth Science and Disaster Resilience (NIED)

Address:
3-1 Tennodai, Tsukuba, Ibaraki 305-0006, Japan

Brief Career:
2017- Research Fellow, NIED

Selected Publications:
• T. Yamada, H. Aoyama, and H. Ueda, "Relationship between infrasound-derived and buoyancy-derived eruption plume volume estimates," Bulletin of Volcanology, Vol.80, No.9, Article 71, 2018.
• T. Yamada, H. Aoyama, T. Nishimura, M. Iguchi, and M. Hendrasto, "Volcanic eruption volume flux estimations from very long period infrasound signals," Geophysical Research Letters, Vol.44, No.1, pp. 143-151, 2017.
• T. Yamada, H. Aoyama, T. Nishimura, H. Yakiwara, H. Nakamichi, J. Oikawa, M. Iguchi, M. Hendrasto, and Y. Suparman, "Initial phases of explosion earthquakes accompanying Vulcanian eruptions at Lokon-Empung volcano, Indonesia," J. of Volcanology and Geothermal Research, Vol.327, pp. 310-321, 2016.

Academic Societies & Scientific Organizations:
• Volcanological Society of Japan (VSJ)
• Japan Geoscience Union (JpGU)
• International Association of Volcanology and Chemistry of the Earth's Interior (IAVCEI)

Name:
Hideki Ueda

Affiliation:
Chief Researcher, National Research Institute for Earth Science and Disaster Resilience (NIED)

Address:
3-1 Tennodai, Tsukuba, Ibaraki 305-0006, Japan

Academic Societies & Scientific Organizations:
• Volcanological Society of Japan (VSJ)
• Seismological Society of Japan (SSJ)

Name:
Toshiya Mori

Affiliation:
Associate Professor, Geochemical Research Center, Graduate School of Science, The University of Tokyo

Address:
7-3-1 Hongo, Bunkyo-ku, Tokyo 113-0033, Japan

Brief Career:
1994- Research Associate, School of Science, The Uniersity of Tokyo
1999-2000 Visiting Scientist at Los Alamos National Laboratory
2004- Associate Professor, Graduate School of Science, The University of Tokyo

Selected Publications:
• T. Mori and M. Burton, "The SO_2 camera: A simple, fast and cheap method for ground-based imaging of SO_2 in volcanic plumes," Geophysical Research Letters, Vol.33, L24804, 2006.

Academic Societies & Scientific Organizations:
• Volcanological Society of Japan (VSJ)
• International Association of Volcanology and Chemistry of Earth's Interior (IAVCEI)
• Geochemical Society of Japan (GSJ)

Name:
Toshikazu Tanada

Affiliation:
National Research Institute for Earth Science and Disaster Resilience (NIED)

Address:
3-1 Tennodai, Tsukuba, Ibaraki 305-0006, Japan

Brief Career:
1987- Hot Springs Research Institute of Kanagawa prefecture
2010- NIED

Selected Publications:
• "Seismicity in the northeast area of Izu Peninsula, Japan, comparing with three dimensional velocity structure and with temperature distribution of geothermal water," Tectonophysics, Vol.306, Issues 3-4, pp. 449-460, 1999.

Academic Societies & Scientific Organizations:
• Volcanological Society of Japan (VSJ)
• Seismological Society of Japan (SSJ)